Proceedings of the ASME 2017 36th International Conference on Ocean, Offshore and Arctic Engineering
OMAE2017
June 25-30, 2017, Trondheim, Norway

OMAE2017-61252

NUMERICAL STUDY OF A MOORED STRUCTURE IN MOVING BROKEN ICE DRIVEN BY CURRENT AND WAVE

Biao Su
SINTEF Ocean
Trondheim, Norway
Email: biao.su@sintef.no

Karl Gunnar Aarsæther
SINTEF Ocean
Tromsø, Norway
Email: karl.gunnar.aarsather@sintef.no

David Kristiansen
SINTEF Ocean
Trondheim, Norway
Email: david.kristiansen@sintef.no

ABSTRACT

This paper presents a numerical model intended to simulate the mooring load and the dynamic response of a moored structure in drifting ice. The mooring lines were explicitly modelled by using a generic cable model with a set of constraint equations providing desired structural properties such as the axial, bending and torsional stiffness. The 6 degrees-of-freedom (DOF) rigid body motions of the structure were simulated by considering its interactions with the mooring lines and the drifting ice. In this simulation, a fragmented ice field of broken ice pieces can be considered under the effects of current and wave. The ice–ice and ice–structure interaction forces were calculated based on a viscoelastic-plastic rheological model. The hydrodynamic forces acting on the floating structure, mooring line and drifting ice were simplified and calculated appropriately. The present study, in general, demonstrates the potential of developing a full numerical model for the coupled analysis of a moored structure in a broken ice field with current and wave.

INTRODUCTION

The use of moored structures in ice represents a promising solution for marine operations in Arctic and Sub-Arctic areas, in particular for the drilling, storage, production and offloading of hydrocarbons. Data from full-scale experiences (see e.g. [1]) and model basin experiments (see e.g. [2-5]) have been used for studying moored structures in ice. Mooring loads and structural response are usually reported in full-scale and model-scale tests of moored structures in ice. Back-calculation of ice actions have been performed by considering the ice force as the unknown in the equations of dynamic equilibrium for moored structures (see e.g. [6-9]).

Numerical studies of moored structures in ice have been focusing on either broken ice, level ice, rubble or ridges, among which the broken or managed ice is perhaps the most relevant ice condition for prospective petroleum industry operations in the Arctic. Incoming ice will often be managed by assisting icebreakers, hence only smaller ice floes will interact with the moored structure. Murray and Spencer [10] used model test data to estimate inertial and damping coefficients caused by broken ice and a discrete element model to calculate ice forces on a turret moored tanker without inertial and damping contributions. A discrete element model was also developed by Hansen and Løset [11-12]. Their model was compared with the model tests of a turret moored ship described by Løset et al. [2]. A different approach was chosen by Sayed et al. [13]. They described broken ice as a cohesionless Mohr-Coloumb material and compared simulations against full-scale data from a conical drilling unit, named Kulluk [1]. Metrikin et al. [14] presented a novel numerical model for the simulation of a dynamic positioning (DP) vessel in managed ice which uses a physics engine for collision detection and contact force computation. In their model, a mooring system can also be implemented as external forces acting on the vessel.

Due to the complexity of modelling interactions between mooring line, moored structure and drifting ice, previous numerical studies have been focusing on the ice actions, while

the mooring part is often simplified. In this paper, we present a numerical model intended to simulate the mooring load and the dynamic response of a moored structure in broken ice. The mooring lines were explicitly modelled by using a generic cable model with a set of constraint equations providing desired structural properties such as the axial, bending and torsional stiffness. The 6 degrees-of-freedom (DOF) rigid body motions of the structure were simulated by considering its interactions with the mooring lines and the drifting ice. In this simulation, a fragmented ice field of broken ice pieces can be considered under the effects of current and wave. The ice–ice and ice–structure interaction forces were calculated based on a viscoelastic-plastic rheological model [15]. The hydrodynamic forces acting on the floating structure, mooring line and drifting ice were simplified and calculated appropriately. The present study, in general, demonstrates the potential of developing a full numerical model for the coupled analysis of a moored structure in a broken ice field with current and wave.

The full-scale experience with the Kulluk structure, provides the best source of data for most considerations related to moored structure in various pack ice conditions [1]. Therefore, the Kulluk structure was selected as a prototype for the present numerical study and the numerical simulation results were compared with the relevant full-scale data. The mooring load is a result of the structural response and it differs from the ice load acting on the structure. This aspect was investigated by the numerical model. Waves are often neglected in numerical studies of ice–structure interactions. A simplified wave force model was applied by the authors in a previous study for simulating wave-driven impact of an ice floe on a circular cylinder [16]. In the present study, wave forces were also considered in ice–ice and ice–structure interactions. However, there is no published data on the wave effects in such condition. This aspect still remains for further analysis.

MATERIALS AND METHODS

The FhSim Framework

FhSim is a time-domain simulation tool that has been under constant development at SINTEF Fisheries and Aquaculture AS (recently named SINTEF Ocean) since 2006, and has served as the primary platform for software development through a series of research projects [17]. In most of these projects, the main role of FhSim has been to represent a framework for developing and numerically solving mathematical models based on Ordinary Differential Equations (ODEs) in the time domain. Model development in FhSim is modular, where complex systems are modelled as a collection of interconnected sub-models. When using FhSim, experts may focus on their special field of competence while taking advantage of verified models made by experts within other fields.

In the present study, the FhSim framework was used for developing ice–ice and ice–structure interaction models. The existing simulation objects in FhSim were also used for modelling sea environments and the mooring components.

Sea Environment

FhSim contains implementations of sea environments providing realizations of wave fields (both regular and irregular), and facilitating queries for time dependent and spatial properties such as:

- Wave elevation on a specified point on the water surface
- Wave induced pressure at a specified point in the water volume
- Wave induced particle velocity and acceleration at a specified point in the water volume
- Ambient current velocity at a specified point in the water volume
- Sea depth at a specified horizontal position

The sea environments support both Airy and Gerstner wave theories and realization of JONSWAP and ISSC wave spectra. The interface to the sea environment objects is generalized to allow different sea state and wave theories to be used without changes to the other simulation models.

In the present study, the wave field was defined explicitly by the sea environment model in FhSim, which was assumed to be undisturbed by the ice floes and a moored structure.

Mooring Line

The mooring lines were modelled by using a generic cable model in FhSim. Both ends of the cable need to be attached to either another sub-model (e.g. a moored structure) or to a fixed point in space (e.g. an anchor point), as this will define both the initial states of the cable and the manner in which the cable will interact with the other components in the system.

Although the cable model in FhSim is essentially a collection of interconnected rigid bar elements exhibiting rigid body motion, they can be equipped with a selection of constraint equations providing desired structural properties such as bending, axial, and torsional stiffness, or contact detection and response. Each rigid bar element in the cable takes compression, but since a cable will consist of several elements the cable will be allowed to buckle under compression forces. The constraint equations are applied to the connections between elements and actively regulate the relative distance and orientation between adjacent elements through an elastic version of the Baumgarte stabilization method [18]. A thorough description of the theoretical and mathematical background for the cable model in FhSim can be found in [19].

Contact Detection and Contact Force Calculation

In the simulation of ice–ice and ice–structure interactions, determining the contact surfaces between interacting ice floes and structures at each time step is a critically important and time consuming calculation. An efficient 3D contact detection

algorithm, called the fast common-plane (FCP) method [20], was used in the present numerical model.

Herein, a common plane (CP) is a plane that, in some sense, bisects the space between the two contacting particles [21]. If the two particles are in contact, then both will intersect the CP, and if they are not in contact, then neither intersects the CP. As a result of using CP, the expensive particle-to-particle contact detection problem reduces to a much faster plane-to-particle contact detection problem. Once the CP is established between two particles, the normal to the CP defines the direction of the contact normal, which in turn defines the direction of the normal contact force between the two particles. As compared with the conventional CP algorithms, the FCP approach recognizes that a common plane has identifying characteristics, which dramatically reduce the search space for the common plane. A thorough description of the FCP approach can be found in [20].

When a CP is found and the two ice floes are intersecting (see e.g. Figure 1), the depth of overlap (δ_c) and the intersection area (A_c) can be determined by solving a simple segment–plane interaction problem. Multiple contacts are allowed in the simulation of ice–ice and ice–structure interactions and a viscoelastic-plastic rheology is applied at all contacts. Hence the normal contact force at time step p, $F_n^c(t_p)$, is expressed as:

$$F_n^c(t_p) = -k_{ns}\delta_c - k_{nv}v_n \tag{1}$$

where k_{ns} is the normal elastic stiffness; k_{nv} is the normal viscous damping coefficient; v_n is the relative velocity (between the two contacting objects) in the normal direction. The magnitude of the normal contact force is controlled by a plastic limit expressed as:

$$\left|F_n^c(t_p)\right| \le -\sigma_c A_c \tag{2}$$

where σ_c is taken to be the uniaxial compressive strength of ice.

The tangential contact force at time step p, $F_t^c(t_p)$, is expressed as:

$$F_t^c(t_p) = F_t^c(t_{p-1}) - k_{ts}v_t\Delta t \tag{3}$$

where $F_t^c(t_{p-1})$ is the tangential contact force at time step $p-1$; k_{ts} is the tangential elastic stiffness; v_t is the relative velocity in the tangential direction; Δt is the time step. The magnitude of the tangential contact force is controlled the Coulomb limit expressed as:

$$\left|F_t^c(t_p)\right| \le -\mu F_n^c(t_p) \tag{4}$$

where μ is the frictional coefficient.

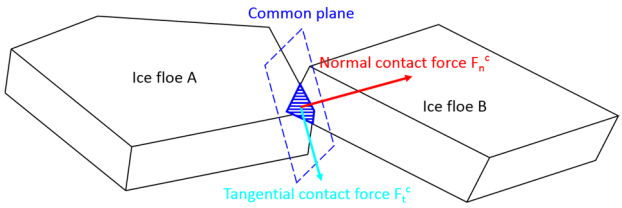

Figure 1. Illustration of the common plane and the normal and tangential contact forces between two interacting ice floes.

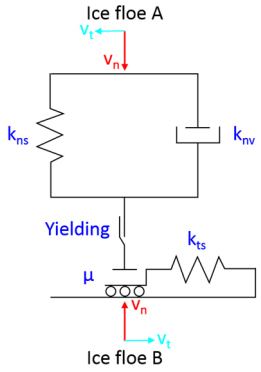

Figure 2. Illustration of the ice–ice (and ice–structure) interaction force model [15].

Kinematics of the Ice Floe and the Structure

The dynamic responses of the ice floe and the structure in current and wave were obtained from the solution of the 6×6 linear system, derived by applying Newton's second law in the body-fixed frame:

$$\sum_{j=1}^{6}\left[(M_{ij}+A_{ij})\ddot{r}_j + B_{ij}\dot{r}_j + C_{ij}r_j\right] = F_i, \quad i = 1,\ldots,6 \tag{5}$$

where M_{ij} are the components of the generalized mass matrix; A_{ij}, B_{ij} and C_{ij} are the 6×6 added-mass, damping and restoring coefficients, respectively; F_i are the components of the excitation forces.

Radiation Forces

The added mass and damping coefficients of the ice floes and the structure were calculated by WAMIT [22] in the frequency domain. The present numerical model employs a time-domain formulation in order to couple the structure to the mooring lines and to incorporate the ice floe impact forces, which requires a time-domain formulation of the frequency-dependent hydrodynamic coefficients. The added mass and damping forces from frequency-domain WAMIT data were transferred to the time domain by application of a linear system adaptation to the convolution integral of Cummin's equation [23] as proposed in [24]. For a combination of degrees of freedom (DOF) i and j, the force takes the form of the equation:

$$F_h(t)_{ij} = -A_{ij}\ddot{v}_{ij} + \int_0^t K_{ij}(t-t')v_{ij}(t')dt' \tag{6}$$

where the frequency response of the convolution integral is the complex function [25]:

$$K_{ij}(jw) = B_{ij}(jw) + jw\left(A_{ij}(jw) - A_{\inf ij}\right) \quad (7)$$

The convolution integral is then replaced by a time dependent force $\mu_{ij}(t)$, which is the output of a linear system selected to reproduce the frequency response of $K_{ij}(jw)$:

$$F_h(t)_{ij} = -A_{ij}\ddot{v}_{ij} + \mu_{ij}(t) \quad (8)$$

$$\dot{\xi}_{ij} = A'_{ij}\,\xi_{ij} + B'_{ij}\,v_j \quad (9)$$

$$\mu_{ij} = C'_{ij}\,\xi_{ij} + D'_{ij}\,v_j \quad (10)$$

The size of the linear system state $\boldsymbol{\xi}$, and the matrices $\mathbf{A'}$, $\mathbf{B'}$, $\mathbf{C'}$ and $\mathbf{D'}$ are selected by fitting the system parameters to $K_{ij}(jw)$ (see e.g. Figure 3). In the present study, the Vector Fitting [26-28] method was used to select the system matrices for each degree of freedom combination with a common $\boldsymbol{\xi}$ size of 8. Only the radiation forces where $i = j$ were included due to the high level of symmetry of the Kulluk structure and the simplified ice floe geometry and to reduce computational complexity. The force $\mu_{ij}(t)$ applied on each ice floe was scaled by its actual area compared to the ice floe geometry analyzed in WAMIT to account for the variations in ice floe shapes.

The above mentioned technique is often referred as a state-space representation [24] of the radiation forces, which is well suited for an efficient time-domain simulation.

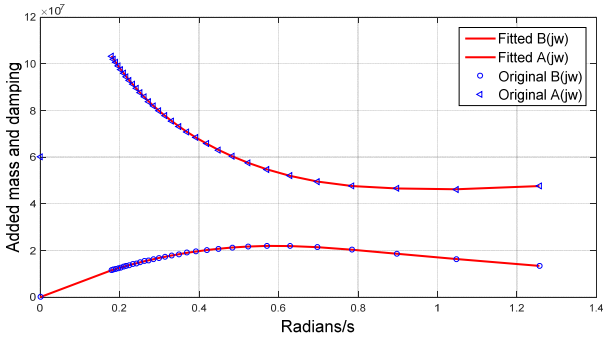

Figure 3. Original frequency-dependent added mass and damping coefficients (WAMIT data) for the heave response of the Kulluk structure, plotted with the reconstructed values from the complex fitted $K_{ij}(jw)$ function.

Excitation forces

The excitation forces on a relatively small body in wave (the characteristic cross-sectional dimension of the ice floe is smaller than 1/5 of the wavelength considered in the present study) can be written as [29]:

$$F_i^p = -\iint_S p n_i ds + \sum_{j=1}^{3} A_{ij} a_{ij}, \quad i = 1,2,3 \quad (11)$$

where p is the pressure in the undisturbed wave field and $\mathbf{n} = (n_1, n_2, n_3)$ is the unit vector of normal to the body defined to be positive into the fluid. The integration is over the wetted surface of the body. Further, a_1, a_2 and a_3 are the acceleration components along the x-, y- and z-axes of the undisturbed wave field and are to be evaluated at the geometrical mass center of the body.

The first term in Equation (11) is the Froude-Kriloff force. The second term physically represents the fact that the undisturbed pressure field is changed due to the presence of the body (diffraction force). It should be noted that Equation (11) only calculates the forces. The resulting moments can also be obtained by the integration over the wetted surface of the body, and the 6-DOF diffraction forces can be calculated using the velocity potentials due to forced motion of the body (added mass and damping) instead of the diffraction potential, for details see [29] and [30].

In addition to the Froude-Kriloff and diffraction forces, the viscous drag force is calculated using Morison's equation:

$$\mathbf{F}^v = \frac{1}{2}\rho C_d A_d \left|\mathbf{V_w} - \mathbf{V_i}\right|(\mathbf{V_w} - \mathbf{V_i}) \quad (12)$$

where ρ is the water density; C_d is the drag coefficient (≈ 1.0); A_d is a reference area (e.g. the cross-sectional area of the body perpendicular to the flow direction); $\mathbf{V_w}$ is the wave-induced particle velocity; $\mathbf{V_i}$ is the velocity of the ice floe.

Furthermore, the Coriolis effect is taken into account when solving the 6-DOF equations of motions in the body-fixed frame. Therefore the expression for the force components in Equation (5) can be written as:

$$\mathbf{F} = \mathbf{F^p} + \mathbf{F^v} + \mathbf{F^{Cor}} + \mathbf{F^c} \quad (13)$$

where $\mathbf{F} = (F_1, F_2, F_3, F_4, F_5, F_6)$ is the total external force acting on the ice floe; $\mathbf{F^p}$ is the Froude-Kriloff and diffraction forces; $\mathbf{F^v}$ is the viscous drag force; $\mathbf{F^{Cor}}$ is the Coriolis force which is a fictitious force induced by a non-uniformly rotating frame (i.e. the body-fixed frame) relative to the inertial frame (for details see e.g. [31]); $\mathbf{F^c}$ is the ice–ice and ice–structure interaction force.

SIMULATION SETUP

The Kulluk structure was selected as a prototype for the present numerical study. Monitoring of ice conditions and measurements of ice forces have provided a comprehensive and unique set of data from the full-scale experience with the Kulluk structure. The monitoring included records of ice cover conditions as well as descriptions of ice management operations. The ice forces were measured using the tension values on the mooring lines. Wright [1] carried out a comprehensive analysis of the observations and measurements. He summarized ice loading episodes in a manner that clearly links ice forces to ice conditions, ice management activities, and the mode of ice interaction with the structure. The present simulations address the categories of "tight" managed ice and managed ice with "good ice clearance" which were identified by Wright [1].

The Kulluk Structure

Figure 4 shows the numerical model of the Kulluk structure with a twelve-line mooring system. The main dimensions of Kulluk were found in [1] and given by Table 1. As no information on the location of the Kulluk's center of gravity was available, it was assumed to be at the geometric center of its near-circular hull, and at the same elevation as its full-displacement waterline [32].

The mooring system was attached below the waterline at a radial distance of 18 m from the hull center (the location of the full-scale fairleads). The mooring lines were assumed to be exactly 30° apart and of equal length. The main properties of individual mooring lines were found in [32] and given by Table 2. In the numerical model, an effective elastic modulus of 67.5 GPa was used to model the full-scale line stiffness which is expressed as:

$$k = EA / l \tag{14}$$

where E is the effective elastic modulus; A and l are the cross-sectional area and the length of the mooring line, respectively.

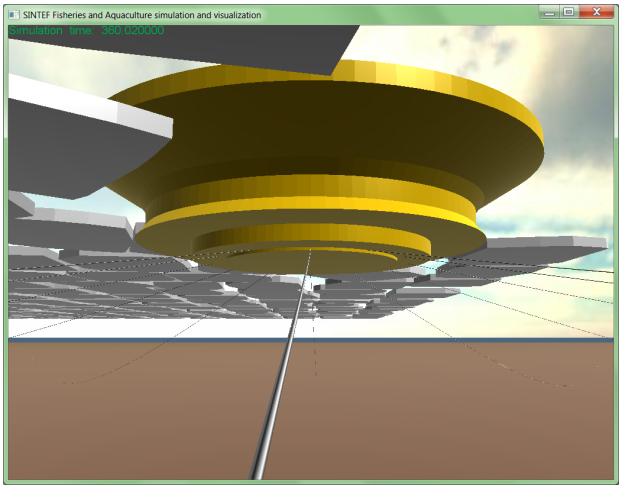

Figure 4. The simulated Kulluk structure with a twelve-line mooring system.

Table 1. Dimension of the Kulluk structure in full scale [1].

Draft	12.5 m
Diameter at deck	81 m
Diameter at waterline	70 m
Diameter at hull bottom	62 m
Displacement	28,000 t
Cone angle	31.4 °

Table 2. Properties of the Kulluk mooring line in full scale [32].

Diameter	88.9 mm
Unit weight (Dry)	33.78 kg/m
Unit weight (Submerged)	28.00 kg/m
Length	917 m
Depth	52 m
Line stiffness	456.65 kN/m
Breaking load	5.1 MN

The Broken Ice Field

Figure 5 shows an example of the simulated broken ice filed driven by current and wave, in which the ice floes were randomly formed with polygonal shapes. The managed ice fragment sizes observed were typically 20 m to 40 m [1]. For the simulation of "tight" managed ice, the floe sizes were taken from a uniform random distribution between 30 m and 40 m, covering an area of 1.2 km by 2.0 km which was confined at the boundaries perpendicular to the drift direction. For the simulation of managed ice with "good ice clearance", the floe sizes were taken from a uniform random distribution between 20 m and 30 m, covering an area of 0.24 km by 2.0 km with contact-free boundaries, in which case the ice floes were, as shown in Figure 6 and [1], drifting in an unconstrained manner and easily cleared around the structure.

In the present study, the thickness of each floe was taken from a uniform random distribution between 2.5 m and 2.7 m, which yielded a mean ice thickness of 2.6 m. This setup referred to a specific ice thickness category defined in [1]. In addition, three different ice concentrations (50%, 70% and 90%) and one current velocity (0.4 m/s) were considered.

The dramatic attenuation of short waves in the marginal ice zone (MIZ) was confirmed by several field experiments. This is the reason why ocean waves typically have not been taken into account when considering ice loads on offshore structures. As there was no wave records available in [1], only a long period wave ($T = 20$ s) which tends to be less attenuated by ice [33] was considered for a comparative study.

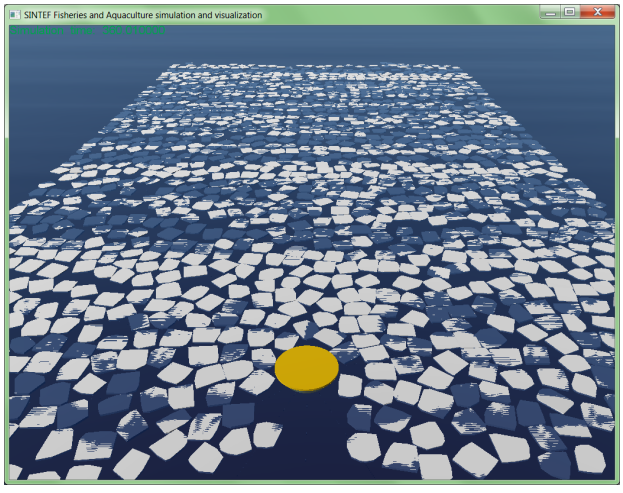

Figure 5. A simulated broken ice field (1.2 x 2.0 km) driven by current and wave ("tight" setup).

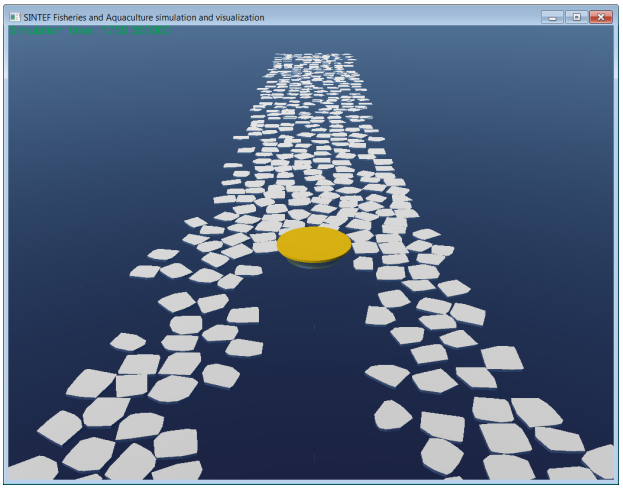

Figure 6. A simulated broken ice field (0.24 x 2.0 km) with free boundaries and driven by current ("good ice clearance" setup).

Ice–Ice and Ice–Structure Interactions

According to the previous numerical studies [15, 34, 11, 12, 35], the parameters of the viscoelastic-plastic rheology need to be adjusted in order to fit the ice floe kinematics and ice–structure interaction forces. The normal elastic stiffness is in principle related to the elastic modulus of ice, and found to be of the order of the elastic modulus multiplied by the ice thickness in a collision between two equally sized disks. The normal viscous damping coefficient and the tangential elastic stiffness are determined from the normal elastic stiffness.

In the present study, a series of simulations were performed, varying the contact parameters. The values of the parameters yielding the best results are given in Table 3. These values were used for the simulations which are presented in the following. The same contact parameters were used for both ice–ice and ice–structure interactions.

Table 3. Values of the contact parameters used in the simulations.

Normal elastic stiffness	1.3 MN/m
Normal viscous damping coefficient	2.6 MN·s/m
Tangential elastic stiffness	0.78 MN/m
Compressive strength	2.5 MPa
Frictional coefficient	0.3

SIMULATION RESULTS

Figure 7 shows an example of the simulated time series of the ice forces, while the corresponding mooring loads (total horizontal loads from the 12 mooring lines) and horizontal offsets of the Kulluk structure are given in Figure 8 and Figure 9, respectively.

By comparing Figure 7 with Figure 8, it can be seen that the time series of the ice forces are generally similar to the mooring loads. However, it is also evident that the simulated ice forces have higher individual peaks than the mooring loads, which was attributed to some individual ice floe impacts that were short in duration. For example, the first impact of the ice floe on the structure caused a rapid rise in the force, and in a very short time the ice floe was diverted and cleared the structure. The individual ice floe impact force was investigated in a previous study by the authors [16], which will not be further discussed in the present paper.

Figure 9 shows an example of the simulated time series of the horizontal offsets of the structure. This result is well below the offset tolerances (1 to 3 m over a 20 to 60 m operating range [1]). However, the dynamic response of the structure and the resulting offset are highly dependent on the mooring stiffness. As there was only one mooring stiffness (i.e. the line stiffness given in Table 2) used in the present simulations, this discussion is not taken any further either.

The mooring load induced by ice–structure interactions will be discussed in the present paper. Therefore, the direct current and wave loads (see e.g. the very beginning part of the mooring load time series shown in Figure 8) will be excluded from the simulation results that are presented in the following. As there were more boundary effects when the structure was entering the broken ice field, the first 1500 s of the time series will also be excluded in the following analysis. Therefore, each time series analyzed covered an ice floe area of about 1 km in distance.

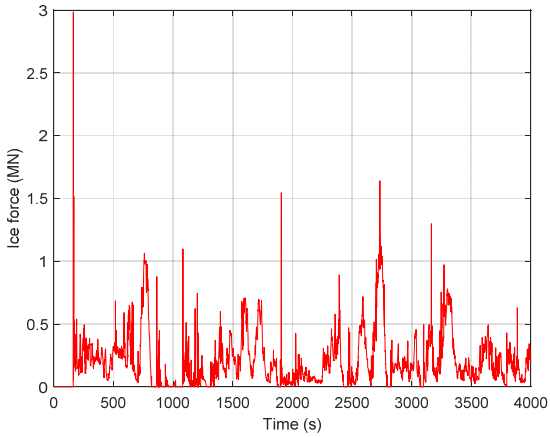

Figure 7. A simulated time series of the ice forces (Ice concentration: 70% (tight); Current velocity: 0.4 m/s).

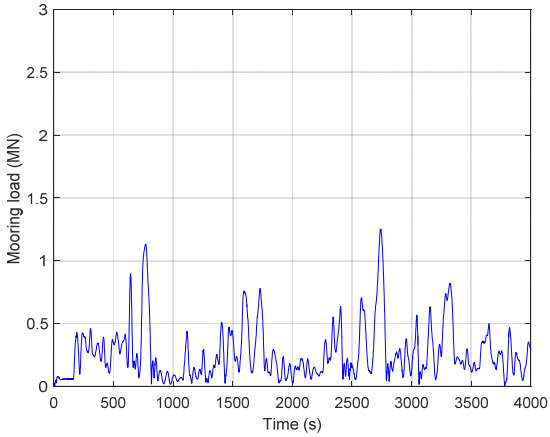

Figure 8. A simulated time series of the mooring loads (Ice concentration: 70% (tight); Current velocity: 0.4 m/s).

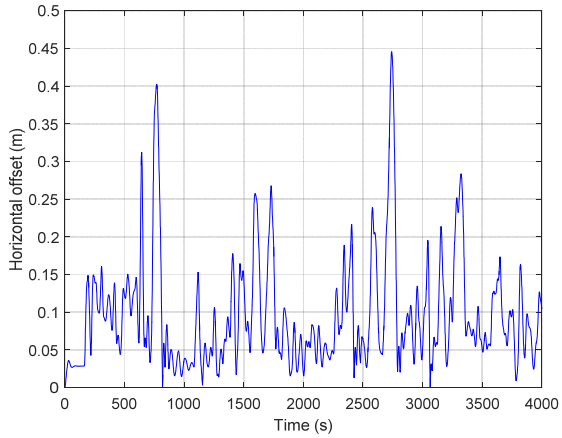

Figure 9. A simulated time series of the horizontal offsets of the structure (Ice concentration: 70% (tight); Current velocity: 0.4 m/s).

DISCUSSIONS

Ice Interaction Modes

In the analysis of Wright [1], the ice interaction events where "good ice clearance" was seen around the Kulluk were treated separately from the situations involving "tight" managed ice conditions with poor clearance, or those involving ice pressure. These two types of events gave rise to different ice interaction behaviors and in turn, different load levels.

Figure 10 compares the simulation results with full-scale data, where the simulated ice floes were in the same ice thickness category (2.5 to 2.7 m) with the full-scale measurements. Both the measured and the simulated plots are the maximum load values during certain ice interaction events. The comparison shows that the simulation results with the "good ice clearance" setup are close to the average level of the full-scale data with "good ice clearance", while the simulation with the "tight" setup are slightly higher than the upper bound of the full-scale data with "good ice clearance" and tends to be in the average level of the full-scale data in "tight" managed ice.

The "tight" managed ice with the pressure from converging ice cover was not considered in the present study. However, a confined ice cover may also give rise to such pressure conditions. In that case, ice accumulating in front of the structure formed a relatively stationary zone of compacted floes, which would cause a considerable rise in the force. The compacted floes might also clear round the structure and accumulate again (see e.g. in Figure 11), which would cause a fluctuation of the forces (see e.g. in Figure 8).

Figure 12 shows the power spectrum of a simulated time series of the mooring load, in which the low-frequency components were associated with the above mentioned accumulating and clearing process within the ice floes, while the high-frequency components drew into the natural frequency of the structure.

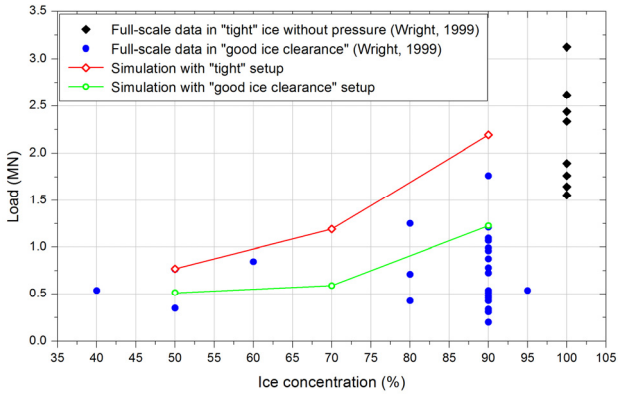

Figure 10. Plot showing a comparison between the simulation results and full-scale data [1].

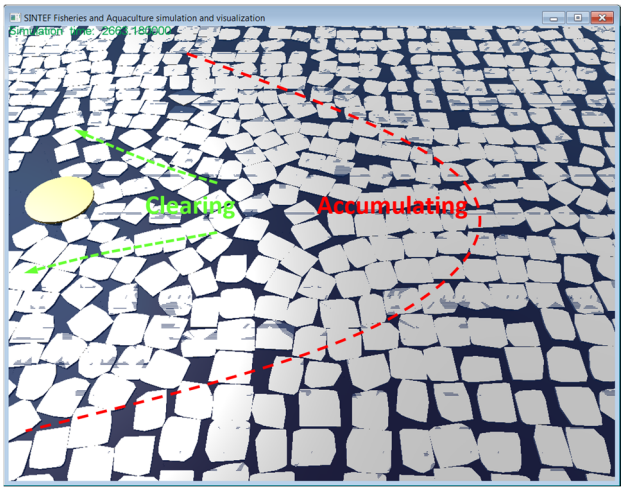

Figure 11. Plot showing the compacted ice floes in front of the structure.

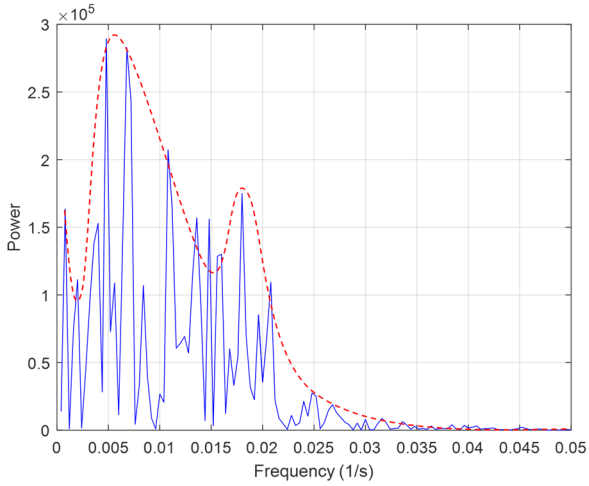

Figure 12. Plot showing the power spectrum of a simulated time series of the mooring load.

Wave Effects in Ice–Structure Interactions

Very few numerical studies have been dealing with the compound effects of waves and ice on structures. Sun and Shen [35], e.g., present a model that was used to determine the loads of a particular type of ice driven by waves and current on circular cylinders. Their model was based on the discrete element method that has been commonly used for simulating

pancake-ice dynamics. Although the load found in their study from pancake ice was much lower than the hydrodynamic counterpart, it was also mentioned that under wave actions other types of ice might produce strong forces on offshore structures.

Figure 13 shows an example of the simulated time series of the mooring loads in moving broken ice driven by current and wave, where a 0.4 m/s current velocity (same as the simulations presented above) and an irregular wave field of 2 m significant wave height and 20 s mean wave period were considered. The direct current and wave loads have been excluded from the time series and the simulation result without wave is also given in Figure 14. By comparing Figure 13 with Figure 14, it is evident that the mooring loads were increased and more fluctuated in waves.

Figure 15 compares the simulation results in different ice concentrations. The compared maximum mooring loads were increased by about 40% to 50% in wave (significant wave height: 2 m; mean wave period: 20 s). A higher increasing rate was also found in lower ice concentrations. However, these effects need to be verified by more data.

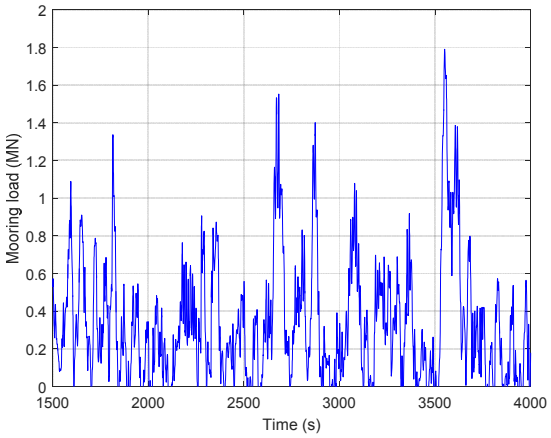

Figure 13. A simulated time series of the mooring loads in moving broken ice driven by current and waves (Ice concentration: 70% (tight); Current velocity: 0.4 m/s; Significant wave height: 2 m; Mean wave period: 20 s).

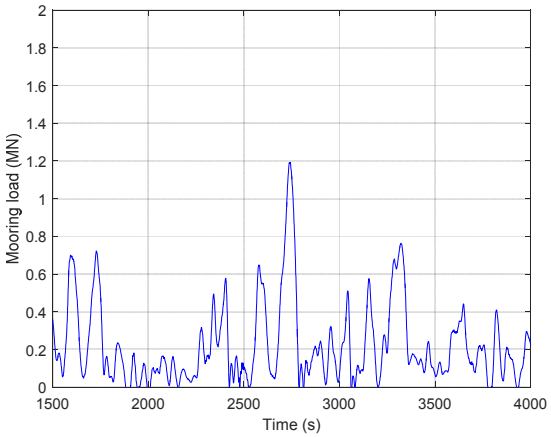

Figure 14. A simulated time series of the mooring loads in moving broken ice driven by current (Ice concentration: 70% (tight); Current velocity: 0.4 m/s).

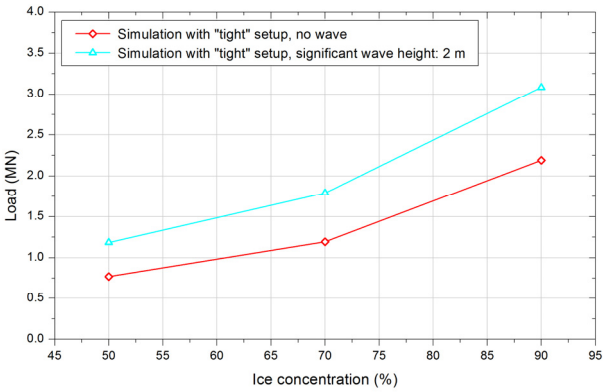

Figure 15. Plot showing a comparison between the simulations without and with wave.

CONCLUDING REMARKS

The present study, in general, demonstrates the potential of developing a full numerical model for the coupled analysis of a moored structure in a broken ice field with current and wave. Based on the comparison with full-scale data, the present numerical model seems to produce realistic results in moving broken ice driven by current. Further investigations are needed regarding the wave effects in ice–structure interactions, the influence of the shape and size of the ice floes on the loads, and the influence of the mooring stiffness on the dynamic response of the structure.

ACKNOWLEDGMENTS

This work is financed by the High North Research Centre for Climate and the Environment (Fram Centre, Tromsø, Norway) through the IFISAW (Ice Floe Interaction with Ships and Waves) project.

REFERENCES

[1] Wright, B., 1999. "Evaluation of full-scale data for moored vessel stationkeeping in pack ice". PERD/CHC Report No. 26-200, National Research Council, Ottawa, Ontario, Canada.

[2] Løset, S., Kanestrøm, Ø. and Pytte, T., 1998. "Model tests of a submerged turret loading concept in level ice, broken ice and pressure ridges". *Cold Reg. Sci. Technol.*, ***27***, pp. 57–73.

[3] Comfort, G., Singh, S., and Spencer, D., 2001. "Moored vessel station-keeping in ice-infested waters: an assessment of model test data for various structures and ship shapes". In Proceedings of the 16th International Conference on Port and Ocean Engineering under Arctic Conditions (POAC 2001), Ottawa, Ontario, Canada.

[4] Bonnemaire, B., Lundamo, T., Evers, K. U., Løset, S. and Jensen, A., 2008. "Model testing of the Arctic Tandem offloading terminal - mooring ice ridge loads". In Proceedings of the 19th IAHR International Symposium on Ice. Vancouver, British Columbia, Canada.

[5] Aksnes, V., 2010. "Model tests of the interaction between a moored vessel and level ice". In Proceedings of the 20th IAHR International Symposium on Ice. Lahti, Finland.

[6] Karulin, E.B., Karulina, M.M., Sazonov, K.E. and Chernetsov, V.A., 2004. "Mathematical model for motion of moored platform interacting with ice". In Proceedings of the 17th IAHR International Symposium on Ice. St. Petersburg, Russia.

[7] Lundamo, T., Bonnemaire, B., Jensen, A., and Gudmestad, O. T., 2008. "Back-calculation of the ice load applying on a moored vessel". In Proceedings of the 19th IAHR International Symposium on Ice. Vancouver, British Columbia, Canada.

[8] Dalane, O., Gudmestad, O.T., Løset, S., Amdahl, J., Fjell, K.H. and Hildèn, T.E., 2008. "Ice tank testing of a surface buoy for Arctic conditions". In Proceedings of the 27th International Conference on Ocean, Offshore and Arctic Engineering (OMAE 2008). Estoril, Portugal.

[9] Murray, J.J., Le Guennec, D.S., Spencer, D., Yang, C.K. and Yang, W., 2009. "Model tests on a SPAR in level ice and ice ridge conditions". In Proceedings of the 28th International Conference on Ocean, Offshore and Arctic Engineering (OMAE 2009). Honolulu, Hawaii, USA,

[10] Murray, J.J. and Spencer, D.S., 1997. "A simulation model for a turret moored tanker in pack ice cover". In Proceedings of the 16th International Conference on Ocean, Offshore and Arctic Engineering (OMAE 1997). Yokohama, Japan.

[11] Hansen, E. and Løset, S., 1999a. "Modelling floating offshore units moored in broken ice: model description". *Cold Reg. Sci. Technol.*, ***29***, pp. 97–106.

[12] Hansen, E. and Løset, S., 1999b. "Modelling floating offshore units moored in broken ice: comparing simulations with ice tank tests". *Cold Reg. Sci. Technol.*, ***29***, pp. 107–119.

[13] Sayed, M., Frederking, R.M.W., and Barker, A. 2000. "Numerical simulation of pack ice forces on structures: a parametric study". In Proceedings of the 10th International Offshore and Polar Engineering Conference (ISOPE 2000), Seattle, USA.

[14] Metrikin, I., Løset, S., Jenssen, N.A., and Kerkeni, S., 2013. Numerical Simulation of Dynamic Positioning in Ice. *Marine Technology Society Journal*, ***47(2)***, pp. 14–30.

[15] Løset, S., 1994. "Discrete element modelling of a broken ice field – Part I: model development". *Cold Reg. Sci. Technol.*, ***22***, pp. 339–347.

[16] Su, B., Aarsæther, K. G. and Kristiansen, D., 2016. "Numerical study of wave-driven impact of a sea ice floe on a circular cylinder". In Proceedings of 35th International Conference on Offshore Mechanics and Arctic Engineering (OMAE 2016), Pusan, South Korea.

[17] Reite, K.J., Føre, M., Aarsæther, K.G., Jensen, J., Rundtop, P., Kyllingstad, L.T., Endresen, P.C., Kristiansen, D., Johansen, V. and Fredheim, A., 2014. "FhSim – Time domain simulation of marine systems". In Proceedings of the 33rd International Conference on Ocean, Offshore and Arctic Engineering (OMAE 2014), San Francisco, California, USA.

[18] Baumgarte, J., 1972. "Stabilization of constraints and integrals of motion in dynamical systems"". *Comput. Meth. Appl. M.*, **1**, pp. 1–16.

[19] Johansen, V., 2007. "Modelling of flexible slender systems for real-time simulations and control applications". PhD Thesis, Norwegian University of Science and Technology, Norway.

[20] Nezami, E.G., Hashash, Y.M.A., Zhao, D. and Ghaboussi, J., 2004. "A fast contact detection algorithm for 3-D discrete element method". *Comput. Geotech.*, ***31***, pp. 575–587.

[21] Cundall, P.A., 1988. "Formulation of a three-dimensional distinct element model-part I: a scheme to detect and represent contacts in a system composed of many polyhedral blocks". *Int. J. Rock Mech. Min. Sci. & Geomech. Abstr.*, ***25(3)***, pp.107–116.

[22] WAMIT, Inc., 2013. "WAMIT user manual, Version 7.0". WAMIT, Inc., Chestnut Hill, MA (2013).

[23] Cummins, W. E., 1962. "The impulse response function and ship motions". No. DTMB-1661. David Taylor Model Basin Washington DC, USA.

[24] Fossen, T. I., 2005. "A nonlinear unified state-space model for ship maneuvering and control in a seaway". *International Journal of Bifurcation and Chaos*, ***15(9)***, pp. 2717–2746.

[25] Pérez, T., and Fossen, T.I., 2008. "Time- vs. frequency-domain identification of parametric radiation force models for marine structures at zero speed". *Modeling, Identification and Control*, ***29(1)***, pp. 1–19.

[26] Gustavsen, B. and Semlyen, A., 1999. "Rational approximation of frequency domain responses by vector fitting". *IEEE Transactions on power delivery*, ***14(3)***, pp. 1052–1061.

[27] Gustavsen, B., 2006. "Improving the pole relocating properties of vector fitting". *IEEE Transactions on Power Delivery*, ***21(3)***, pp. 1587–1592.

[28] Deschrijver, D., Mrozowski, M., Dhaene, T., and De Zutter, D., 2008. "Macromodeling of multiport systems using a fast implementation of the vector fitting method". I*EEE Microwave and Wireless Components Letters*, **18(6)**, pp. 383–385.

[29] Faltinsen, O., 1993. *Sea loads on ships and offshore structures*. Cambridge university press.

[30] Newman, J. N., 1977. *Marine hydrodynamics*. MIT press.

[31] Fossen, T. I., 2011. *Handbook of Marine Craft Hydrodynamics and Motion Control*. Wiley & Sons.

[32] Stanley, J. and Lau, M., 2004. "Design of a mooring system for model testing of a downward breaking moored cone in ice". CNRC Report SR-2005-01, National Research Council, Ottawa, Ontario, Canada.

[33] Ardhuin, F., Sutherland, P., Doble, M. and Wadhams, P., 2016. "Ocean waves across the Arctic: Attenuation due to dissipation dominates over scattering for periods longer than 19 s". *Geophysical Research Letters*, ***43(11)***, pp. 5775–5783.

[34] Løset, S., 1994. "Discrete element modelling of a broken ice field – Part II: simulation of ice loads on a boom". *Cold Reg. Sci. Technol.*, ***22***, pp. 339–347.

[35] Sun, S. and Shen, H.H., 2012. "Simulation of pancake ice load on a circular cylinder in a wave and current field". *Cold Reg. Sci. Technol.*, **78**, pp. 31–39.